

Horseshoe templates with global torsion in a driven laser

G. Boulant,^{*} M. Lefranc,[†] S. Bielawski,[‡] and D. Derozier[§]

Laboratoire de Spectroscopie Hertzienne, URA CNRS 249, Centre d'Études et de Recherches Lasers et Applications, Université de Lille I, F-59655 Villeneuve d'Ascq Cedex, France

(Received 26 December 1996)

We perform a topological analysis of chaotic signals from a Nd-doped fiber laser with pump modulation at different values of the modulation frequency. In this experiment, the system displays chaotic behavior in three regions $C_{1/4}$, $C_{1/3}$, and $C_{1/2}$ of parameter space, located around the subharmonics $\omega_r/4$, $\omega_r/3$, and $\omega_r/2$ of the relaxation frequency ω_r . We observe that the topological structures of the chaotic regimes inside a given region $C_{1/n}$ are described by the same template. However, templates corresponding to different regions display different global torsions θ_g , which we find to be related to the order of the subharmonics by $\theta_g(C_{1/n}) = n - 1$. [S1063-651X(97)09804-8]

PACS number(s): 05.45.+b, 42.65.Sf, 42.55.Wd

I. INTRODUCTION

Template analysis allows a relevant classification and comparison of chaotic attractors according to their topological properties and provides a clear-cut characterization thereof by a set of integer topological indices [1] which are robust with respect to variations in control parameters. In particular, attractors observed experimentally in various fields such as chemistry [2,3], mechanics [4], nuclear magnetic resonance [5], and optics [6–8], have been shown to belong to the same class, namely, that of the Smale's horseshoe with zero global torsion. Let us note, however, that nonhorseshoe dynamics has been reported by Firlé, Natiello, and Eiswirth [9] and that other structures have been predicted to be observable in experiments [10,11].

In this paper, our aim is to use topological analysis in order to study and compare the attractors of a single system (a modulated Nd-doped fiber laser), at different values of a control parameter (the modulation frequency ω). We do this in an experimental situation where chaotic behavior is observed when ω lies near the subharmonics $1/2$, $1/3$, and $1/4$ of the natural relaxation frequency ω_r , the highest linear resonance frequency (see, e.g., [12,13]) of the system.

Let us briefly recall the principle of the method. A chaotic attractor has typically embedded in it a dense set of unstable periodic orbits (see, e.g., [14]) which cannot intersect because of the deterministic nature of the evolution laws. Thus the way the unstable periodic orbits (UPO) are linked together can be characterized using concepts from knot theory, provided the attractor is confined to a three-dimensional (3D) manifold. The existence of a two-dimensional manifold, the *template*, such that all UPO can be placed on it while preserving their invariant linking properties, allows one then to describe concisely the global topological organization of the attractor under study.

The fiber laser (FL) is known to be a possibly high-

dimensional system with many longitudinal modes oscillating simultaneously. Hence, in Sec. II we describe the experimental system and check that topological analysis is applicable by estimating the Lyapunov dimension of the attractors. Then, Sec. III is devoted to the extraction of UPO from experimental data and the computation of their topological invariants. We show there how careful signal processing can greatly help in extracting topological information from noisy time series of finite length and precision. Finally, in Sec. IV, we determine the templates of the different attractors, compare them, and relate them to the values of the modulation frequency. In particular, we show that these templates have a nonzero global torsion, and that this torsion increases by one full turn when the period of modulation increases by $2\pi/\omega_r$. This observation is in close agreement with the theoretical studies of modulated nonlinear oscillators by Gilmore and McCallum [10].

II. THE EXPERIMENTAL SYSTEM

The experimental setup is a Fabry-Pérot laser cavity. The active medium, a 4 m long silica fiber doped with 300 ppm Nd^{3+} , is pumped by a laser diode emitting a single polarized mode at 810 nm. The optogeometrical properties of the fiber make the laser transversally monomode at the operating wavelength $\lambda = 1.08 \mu\text{m}$. However, the large cavity length and the broad inhomogeneous gain profile (100 cm^{-1}) allow some 10 000 longitudinal modes to oscillate simultaneously. In addition, in the absence of polarization selective elements in the cavity, each mode is split into two eigenstates of polarization depending on the birefringence of the fiber [15]. On output, the two polarization eigenstates of the cavity are separated by a polarizing beam splitter combined with a half-wave plate to select the direction of analysis. In typical operating conditions, the low laser threshold allows us to reach pump parameters (i.e., the ratio of the pump power to its value at threshold) up to 5 and to explore a wide range of parameters.

Under modulation of a control parameter, this laser exhibits chaotic oscillations [16], reached via period doubling cascade or quasiperiodicity. In our experiment, we modulate sinusoidally the pump parameter $A(t) = A_0(1 + m \cos \omega t)$

^{*}Electronic address: Guillaume.Boulant@univ-lille1.fr

[†]Electronic address: Marc.Lefranc@univ-lille1.fr

[‡]Electronic address: Serge.Bielawski@univ-lille1.fr

[§]Electronic address: Dominique.Derozier@univ-lille1.fr

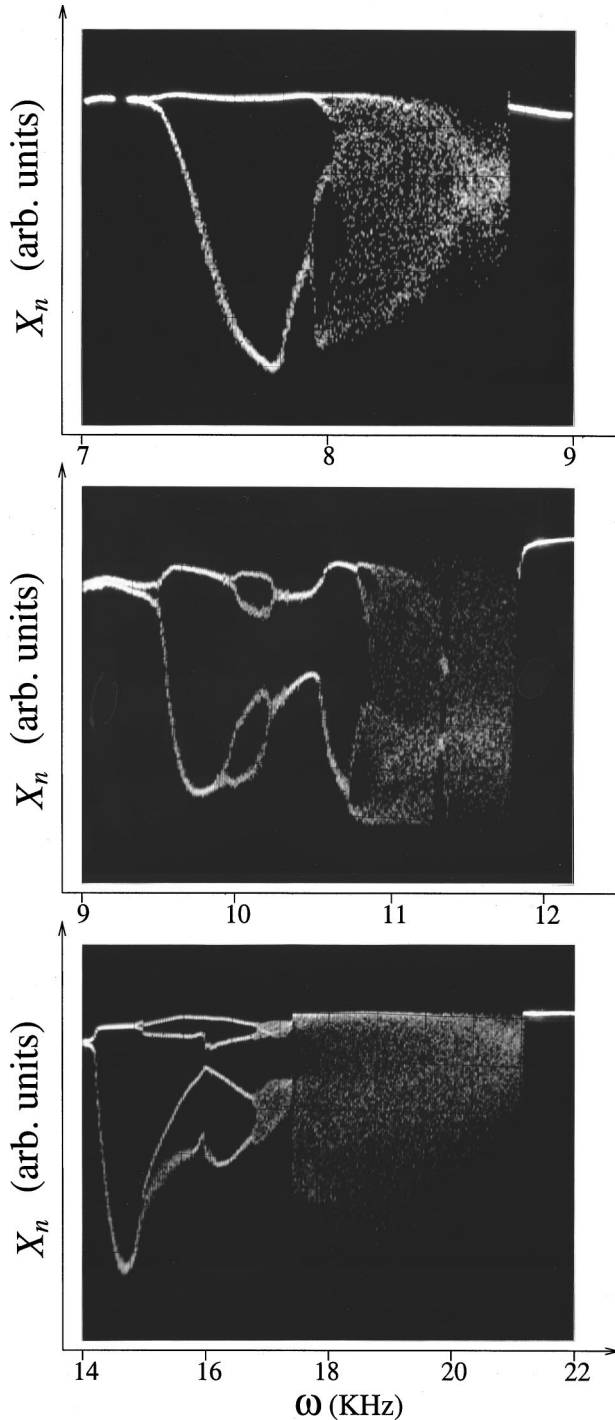


FIG. 1. Experimental bifurcation diagram for increasing modulation frequency. Note the localization of the three chaotic regimes around $\omega_r/4$, $\omega_r/3$, and $\omega_r/2$.

around an average value $A_0=2.7$ with a rate $m=0.6$. The frequency is chosen as a control parameter and swept from 0 to the relaxation frequency ω_r , which, under these conditions, is about 36 kHz. The bifurcation diagram, shown in Fig. 1, displays a sequence of three chaotic windows $C_{1/4}$, $C_{1/3}$, and $C_{1/2}$ located around $\omega_{1/4}\approx 9$ kHz, $\omega_{1/3}\approx 12$ kHz, and $\omega_{1/2}\approx 18$ kHz, respectively. The notations have been chosen to emphasize the harmonic relation between the chaotic frequencies and ω_r

$$\omega_r \approx 2\omega_{1/2} \approx 3\omega_{1/3} \approx 4\omega_{1/4}. \quad (1)$$

TABLE I. Estimated Lyapunov exponents of sample regimes in $C_{1/4}$, $C_{1/3}$, and $C_{1/2}$ regions, given in modulation frequency units. d_L is the Lyapunov dimension defined as $d_L=2+|\lambda_1/\lambda_3|$ according to the Kaplan-Yorke conjecture [29] and is believed to estimate the dimension of the attractor.

Regime	λ_1	λ_2	λ_3	d_L
$C_{1/4}$	0.37	-0.06	-0.57	2.6
$C_{1/3}$	0.34	-0.00	-0.92	2.3
$C_{1/2}$	0.52	-0.03	-0.66	2.7

This bifurcation structure is common in nonlinear oscillators (see, e.g., [10]) except that, in the present case, we do not observe chaotic behavior around the relaxation frequency ω_r .

To verify that, in spite of the great number of degrees of freedom, the dynamics is sufficiently low dimensional so that template analysis can be applied, we have performed Lyapunov exponent estimates for regimes in the three regions using the program DLIA by Briggs [17]. Table I displays the results obtained for three sample regimes. While the numerical values should be taken with caution, especially for the negative exponent (the regimes appear to be much more dissipative than indicated by this analysis), they definitely show that there is only one unstable direction and that three-dimensional volumes are contracted under the action of the flow. This means that most of the dynamical variables relax so quickly that they are enslaved by a few number of collective variables which are confined to a three-dimensional manifold. This motivates the topological analysis carried out in the sequel of this paper, whose relevance will, furthermore, be confirmed by the consistency of the measured topological invariants [18].

III. TOPOLOGICAL ANALYSIS

As complex as it may appear, a strange attractor is a highly organized geometrical object. In particular, it contains an infinite number of unstable periodic orbits (UPO), densely embedded in it (see, e.g., [14]): the neighborhood of any point of the attractor, however small it is, is visited by periodic orbits. As it evolves on a strange attractor, a typical chaotic trajectory visits the neighborhood of a number of these UPO, approaching them along their stable direction and leaving them along the local unstable direction, after an interval of time whose duration depends on how closely the periodic orbit has been approached.

In low-dimensional attractors, the crossing of the neighborhood of an UPO of relatively low period by a chaotic trajectory shows itself clearly in the temporal signal as a burst of almost periodic behavior. This allows one to extract approximations of periodic orbits from experimental time series. Some examples of such sequences, with a high signal to noise ratio, can be found, for instance, in Ref. [7].

Unstable periodic orbits have been recognized as a major tool to analyze chaotic systems. Indeed, they provide a hierarchical approximation of a strange attractor: low-period orbits model the global structure of the attractor, while finer details can be resolved using high-period orbits. One promising and powerful method based on this approach is the

topological analysis proposed by Mindlin *et al.* [1], which proceeds as follows.

Periodic orbits are associated with closed curves in the phase space of the system. When this phase space is three dimensional, these curves can be characterized using the mathematical framework of knot theory (see, e.g., Ref. [19]). The latter associates with a three-dimensional closed curve (or a set of such curves) topological numbers which are invariants with respect to isotopy, i.e., which remain unchanged when the curve is continuously deformed without intersecting itself.

The relevance of these invariants stems from the deterministic nature of chaotic behavior. Indeed the uniqueness theorem (see, e.g., Ref. [20]) implies that a periodic orbit cannot intersect itself or another orbit without violating determinism at the point of intersection. As a result, invariants from knot theory are well defined and are insensitive to deformations induced by modifying a control parameter. For example, the relative placement of a pair (α, β) of unstable periodic orbits can be characterized on its whole domain of existence in parameter space by several topological quantities such as the linking number $lk(\alpha, \beta)$, which indicates how many times α winds around β .

The keystone of topological analysis is that any set of periodic orbits embedded in the attractor is associated to a set of orbits with identical topological invariants on a two-dimensional manifold, called the *template* [21–23,1]. This surface can be viewed as a *knot holder* on which all the periodic orbits extracted from the attractor can be laid down via a continuous deformation without crossing. Thus the template provides a simple and complete description of the global topological organization of the flow.

In this section, we describe the steps we have followed to extract UPO from experimental signals of the FL and to compute their topological invariants. The determination of the corresponding templates will be presented in Sec. IV.

To perform a topological analysis, a time series $X(t)$ has to be embedded in a three-dimensional phase space, so that knot theory can be applied. In Sec. III A, we first describe the particular phase space we have used. Due to the relatively complex nature of the signals coming from the FL, it has been necessary to process them using analog techniques — which we present in Sec. III B — in order to obtain a time series suitable for topological analysis. Indeed, computing the topological invariants of the UPO detected in the time series requires an embedding phase space where orbits are well separated. If two orbits are too close to each other in some region of the attractor, the experimental noise and the slight uncertainty in their precise localization (we use orbits approximating the true UPO) may result in unreliable measurements of their relative positions and, thus, of their linking invariants. In Sec. III C, we briefly review the close-return technique used to extract the unstable periodic orbits from the time series. Last, we classify the detected orbits using symbolic dynamics and compute their topological invariants for chaotic regimes inside the $C_{1/4}$, $C_{1/3}$, and $C_{1/2}$ chaotic regions in Sec. III D.

A. Embedding phase space

As mentioned above, topological analysis requires that the time series $X(t)$ under study be embedded in a 3D phase

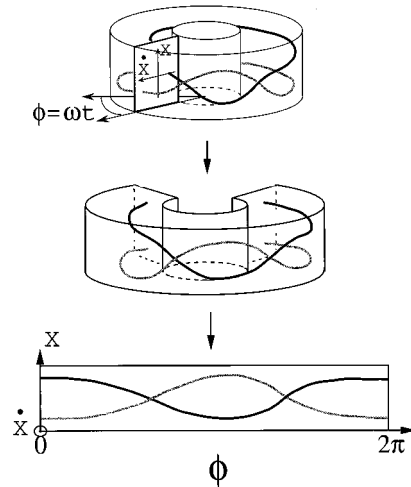


FIG. 2. 3D differential embedding phase space. $X(t)$ is a dynamical variable and ϕ the modulation phase. The topological information (contained in overcrossings and undercrossings) is completely preserved in a plot of X vs ϕ . For example, the two crossings in the latter reflect the fact that each orbit winds one time around the other, which corresponds to a linking number of 1.

space. In our experiments, we have used a phase space with coordinates $[X(t), \dot{X}(t), \phi(t)]$, where $\phi(t) = \omega t \pmod{2\pi}$ is the phase of the period- T modulation. This phase space, which is schematically displayed in Fig. 2, is topologically equivalent to a solid torus $D^2 \times S^1$ (D^2 being the unit disk and S^1 the unit circle). This is a natural geometry for a modulated system, as a Poincaré section of the attractor can be readily obtained by means of a stroboscopic sampling. Moreover, this topology restricts isotopy moves to a smaller class, namely, regular isotopy, and allows one to make use of more powerful invariants, such as the relative rotation rates introduced by Solari and Gilmore [24,25], which provide a finer description of the relative rotation of the UPO than the linking number.

$X(t)$ and its time derivatives are natural variables to describe a dynamical system. There is, however, one more reason for choosing the time derivative $\dot{X}(t)$ as the second coordinate. Indeed, the topological structure of a periodic orbit α of period T_α can then be completely analyzed by plotting its representative time series segment $X_\alpha(t)$, $t \in [t_0, t_0 + T_\alpha]$ as a function of $\phi = \omega t \pmod{2\pi}$ [7]. As illustrated in Fig. 2, this plot can be seen as a projection of the orbit onto the $\dot{X} = 0$ cylinder along the \dot{X} direction, and presents the orbit as a braid on n strands. Topological information is preserved provided that we know at each crossing which of the two strands passes over the other in the 3D space. This is, in fact, trivial since the strand with the greater slope corresponds to the higher value of \dot{X} .

As a result, listing the successive crossings as ϕ increases from 0 to 2π provides an algebraic description of the topological structure of the orbit, from which any topological invariant can be readily computed. As a simple example, computing the linking number of two orbits amounts to counting the number of crossings between the strands of these two orbits in a $X(\phi)$ plot (see the example of Fig. 2).

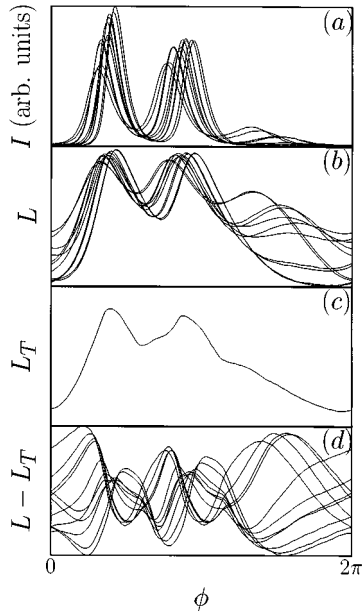


FIG. 3. Enhancement of the topological information of the signal by analog processing. (a) A polarization eigenstate intensity: I . (b) Logarithmic amplification of this signal: $L = \ln(I)$. (c) The unwanted period- T oscillation L_T . (d) The final signal $X = L - L_T$.

Clearly, evaluating this number requires that different strands be well separated, particularly because of the limited resolution of the eight-bit transient digitizer used in the experiments. This is not necessarily so when directly recording a natural variable of the system, for example, the laser intensity. In this case, the signal has to be processed using analog techniques before the topological analysis of digitized data can be carried out.

B. Signal processing

As Fig. 3(a) shows, the intensity I of a polarization eigenstate is not a suitable variable, because it almost completely vanishes during long periods of time. In these regions of low intensity, the different orbits are indiscernible and we cannot determine whether some crossings occur. As advocated in Ref. [26], this problem can be overcome by using a logarithmic amplifier which delivers an output signal $L(t) = \ln(I(t) + I_0)$. Let us note that this procedure, successfully followed in previous topological investigations of the modulated CO_2 laser [7,8], preserves the topological information since $L(t)$ is a monotonic function of $I(t)$.

As can be seen in Fig. 3(b), this first step improves the quality of the signal to some extent but yet does not suffice. Indeed, the resulting signal $L(t)$ displays a strong periodic component at frequency $1/T$ which masks the rest of the dynamics: the signal remains confined to a narrow band around this period- T oscillation. Fortunately, any T -periodic transformation of the form $L(t) \rightarrow L(t) + f(\phi(t))$ does not modify the relative positions of crossings and, hence, leaves isotopy invariants unchanged.

Experimentally, one simple way to proceed is thus to subtract a T -periodic signal $L_T(t) = L_T(\phi(t))$ from $L(t)$, where $L_T(t)$ approximates the unwanted period- T oscillation. In our experiments, we have chosen $L_T(t)$ to be

$$L_T(t) = \frac{\xi_+(\phi(t)) + \xi_-(\phi(t))}{2}, \quad (2)$$

where $\xi_+(\phi(t))$ and $\xi_-(\phi(t))$ are, respectively, the high and low envelopes of $L(t)$ computed from a record of about 1000 modulation periods

$$\xi_+(\phi_0) [\text{resp. } \xi_-(\phi_0)] = \max(\text{resp. } \min)\{L(t); \phi(t) = \phi_0\}.$$

Figure 3(c) displays the L_T correction corresponding to the signal of Fig. 3(b).

This periodic signal is then generated with a programmable synthesizer phase locked on the modulation, and subtracted from the output of the logarithmic amplifier. The final signal, shown in Fig. 3(d), clearly displays the topological information and provides a suitable dynamical variable. In the following, the time series $X(t)$ will, thus, always designate the dynamical variable

$$X(t) = L(t) - L_T(\phi(t)) \quad (3)$$

and the embedding 3D phase space will be the $D^2 \times S^1$ torus $[X(t), \dot{X}(t), \phi(t)]$.

C. Detection of the unstable periodic orbits

The extraction of periodic orbits embedded in the attractor is carried out by applying to time series of $X(t)$ the close-return technique proposed in Ref. [2]. The latter proceeds by looking for time series segments $\{X(t); t \in [t_0, t_0 + pT]\}$ satisfying

$$|X(t + pT) - X(t)| < \varepsilon \quad \text{for } t_0 < t < t_0 + pT. \quad (4)$$

Such a sequence indicates that the trajectory in phase space is shadowing a period- pT orbit and can be used as an approximation of this orbit, as better as ε is smaller.

In our experiments, with a signal to noise ratio in the order of 1%, we have chosen ε to be 5% of the maximum amplitude of $X(t)$ and have narrowed the search to orbits of period pT up to $p = 10$.

Due to ergodicity, an infinitely long chaotic trajectory passes arbitrary close to any UPO. On the contrary, a finite experimental time series can only approach a finite number of periodic orbits. Furthermore, the presence of noise will prevent higher-period orbits to be shadowed over a sufficient interval of time. Therefore, only a relatively small number of orbits can, in practice, be extracted, except when the signal to noise ratio is high. For each attractor we have recorded signals over 10 000 modulation periods, which typically contained some hundred almost periodic sequences, corresponding to about ten distinct UPO for the $C_{1/4}$ and $C_{1/3}$ regions. In the $C_{1/2}$ region, we have observed the chaotic regimes to be much less dissipative than in the two former ones. This adversely affects the detection of the UPO for two reasons: the time needed before entering the neighborhood of a given UPO is significantly increased, and the influence of noise is strengthened. This explains why the results we present for this part of the parameter space are obtained from a smaller number of periodic orbits than for the $C_{1/4}$ and $C_{1/3}$ regimes. We are currently trying to design an alternate detection method to overcome this limitation.

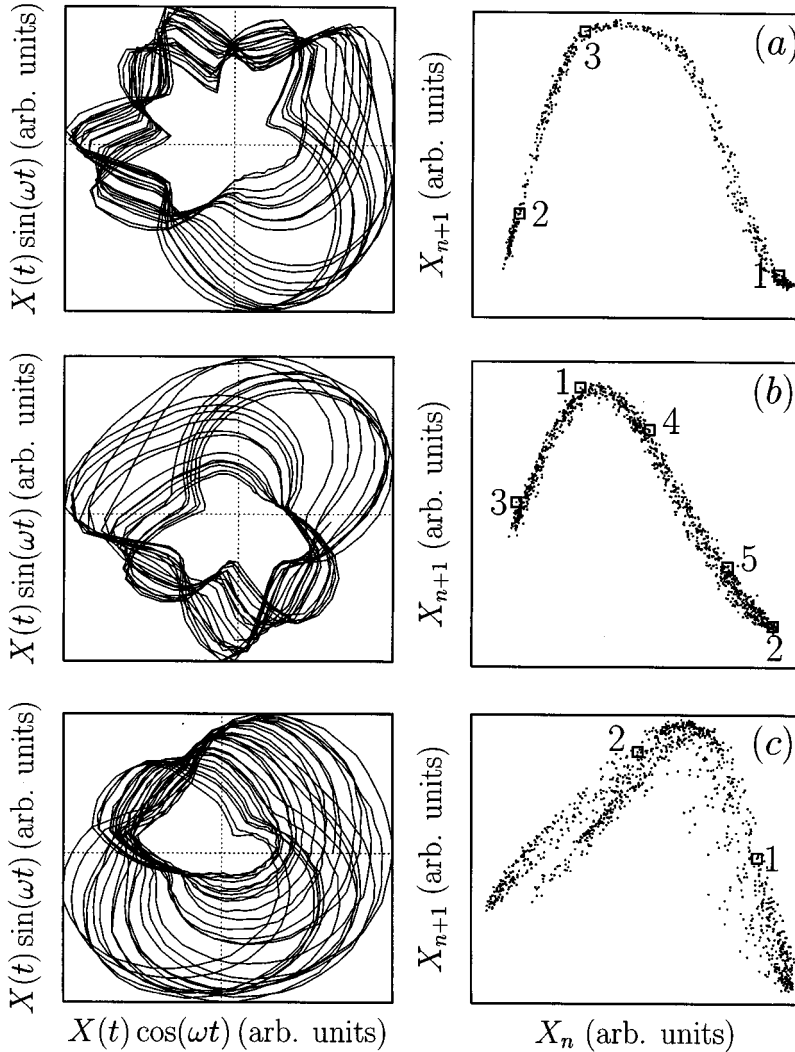


FIG. 4. Two-dimensional projections of attractors (on the left) and their corresponding first return diagram (X_{n+1}, X_n) , where X_n is the stroboscopically sampled variable $X_n = X(\phi_0 + 2n\pi)$. (a) Regime $C_{1/4}$. (b) Regime $C_{1/3}$. (c) Regime $C_{1/2}$. Note that these return diagrams are well approximated by a unimodal map, and can be used to perform a symbolic encoding of the orbits. On diagram (a) is plotted the $xyx = x^2y$ period- $3T$ orbit, on (b) the x^2y^3 period- $5T$ orbit, and on (c) the xy period- $2T$ orbit.

D. Spectrum of periodic orbits and computation of the topological invariants

Template analysis is significantly easier when the extracted periodic orbits can be classified using symbolic dynamics. Symbolic dynamics is a powerful approach of chaotic behavior and proceeds by representing a chaotic trajectory as a sequence of symbols while retaining most of the dynamical information. Most topological investigations, so far, have been carried out in cases where symbolic coding could be obtained by means of 1D first return maps [2,5–7], with the exception of Ref. [8].

For each regime of the FL, the 1D first return diagram (X_n, X_{n+1}) , where the $X_n = X(t_0 + nT)$ are obtained by a stroboscopic sampling, is well approximated by a unimodal map of an interval onto itself: $X_{n+1} = P(X_n)$, as can be seen in Fig. 4. The theory of symbolic dynamics for such maps is well established (see, e.g., Ref. [27]) and thus can be used here to encode periodic orbits.

A unimodal map has a single critical point X_c which separates the regions with positive and negative slope. A pT orbit, identified by p samples $X_1 = X(t_1)$, $X_2 = X(t_1 + T)$, \dots , $X_p = X(t_1 + (p-1)T)$, is encoded by a binary string $s_1 s_2 \dots s_p$, where $s_i = x$ (respectively, y) when $X_i < X_c$ (respectively, $X_i > X_c$). As an example, the period-

$3T$ orbit $\overline{yxx} = \overline{yx^2}$ of a $C_{1/4}$ regime, the period- $5T$ $\overline{yxxyy} = \overline{yx^2y^2} = \overline{x^2y^3}$ of a $C_{1/3}$ regime, and the period- $2T$ \overline{xy} of the $C_{1/2}$ regime are displayed in Figs. 4(a)–4(c). The relevance of this symbolic encoding will fully appear in Sec. IV.

Once the periodic orbits have been extracted and classified according to symbolic dynamics, one can proceed to compute their topological invariants. For each periodic orbit, we have computed its self-linking number and self-relative rotation rates, while pairs of orbits have been characterized by their linking number and relative rotation rates. Note that, with the exception of the linking number, these invariants are available thanks to the toroidal topology of the phase space.

(Self-)linking numbers are determined by counting crossings in $X(\phi)$ plots as described in Sec. III A: the self-linking (respectively, linking) number is simply the sum (respectively, half-sum) of the number of crossings of the orbit with itself (respectively, the other orbit).

As for the relative rotation rates, let us briefly recall that a period- pT orbit α and a period- qT orbit β can be characterized by $p \times q$ relative rotation rates $\{R_{ij}(\alpha, \beta); i=1, \dots, p \text{ and } j=1, \dots, q\}$. If the intersections of α and β with a Poincaré section are labeled $X_1^\alpha, \dots, X_p^\alpha$ and $X_1^\beta, \dots, X_q^\beta$, the R_{ij} relative rotation rate is defined as the

TABLE IV. Linking and self-linking numbers of the UPO extracted from the $C_{1/3}$ regime.

Orbits	T	$2T$	$4T$	$5T_a$	$5T_b$	$6T_a$	$6T_b$	$7T_a$	$7T_b$	$7T_c$	$9T_a$	$9T_b$
$T=y$	0											
$2T=xy$	5	5										
$4T=xy^3$	10	19	29									
$5T_a=xy^4$	12	24	48	48								
$5T_b=xyxy^2$	12	24	48	60	48							
$6T_a=xy^5$	15	29		72	72	73						
$6T_b=xyxy^3$	15	29	58	72	72		73					
$7T_a=xyxyxy^2$	17	33	67	84	83	101	100	100				
$7T_b=xy^6$	17	34	68	84	84		102	118	102			
$7T_c=xyxy^4$	17	34	68	84	84	102				102		
$9T_a=xy^2xyxy^3$	22	43	86	108		130				151	172	
$9T_b=xyxyxy^4$	22	43	87									174

sample regimes. We have observed that inside a single region $C_{1/n}$, topological invariants depend on symbolic sequences only. For example, we have found $lk(y,xy)=7$ for any $C_{1/4}$ -type regime. Since the linking number of two orbits does not depend on control parameters in their whole domain of existence, this gives strong evidence that a given periodic orbit is associated to one and only one symbolic sequence throughout a chaotic region $C_{1/n}$.

On the contrary, two orbits with the same symbolic sequence, but which belong to two different $C_{1/n}$ regions, appear to be different, as shown by their topological properties. For example, we have found that $lk(y,xy)=7$ in the $C_{1/4}$ region but $lk(y,xy)=5$ (respectively, 3) in the $C_{1/3}$ (respectively, $C_{1/2}$) one. As we will see in Sec. IV, this discrepancy is explained by the fact that these regions correspond to three different templates, and thus to three different types of topological organization.

IV. DETERMINATION OF THE TEMPLATES

As we have seen in the preceding section, the first stage of topological analysis yields tables collecting the invariants of orbits and pairs of orbits, from which the global structure of the flow is hard to discern.

To gain more insight into this structure, the organization of the knotted orbits can be modeled by means of a branched 2D manifold, the *template*. The mathematical definition of a template (a.k.a. “knot holder”) has been introduced by Birman and Williams [21]. They have proved that the periodic orbits of a three-dimensional hyperbolic flow exhibiting chaos are in one-to-one correspondence with those of a semiflow defined on the template. The latter is obtained by col-

TABLE V. Linking and self-linking numbers of UPO extracted from the $C_{1/2}$ regime.

Orbits	T	$2T$	$3T$	$4T$	$10T$
$T=x$	0				
$2T=xy$	3	3			
$3T=x^2y$	4	8	8		
$4T=x^2y^2$	5	10	15	15	
$10T=xy^2x^2y^2x^2y$	13				

lapsing the invariant set of the 3D flow along its stable manifold, i.e., by identifying points whose images converge to each other as time goes to infinity. As, for obvious reasons, a periodic orbit intersects neither its stable manifold nor those of other periodic orbits, the topological organization is preserved in the process.

Strange attractors are generally not hyperbolic. In particular, periodic orbits can be created or destroyed as a control parameter is varied. However, existing periodic orbits are linked as in the hyperbolic limit, since their topological invariants do not depend on control parameters, and can be put in correspondence with some periodic orbits of the hyperbolic template. Thus, for experimental systems, the template is still a relevant concept but differ from the mathematical definition by the fact that not all its periodic orbits do have a counterpart in the attractor.

One of the most simple chaotic topological structures is the one described by the horseshoe template, named after the Smale’s horseshoe, a celebrated paradigm of a chaotic dynamical system (see, e.g., Ref. [28]). Figure 5 shows the horseshoe template holding a $3T$ orbit. It is essentially divided into two parts. The most important one models the folding and stretching processes organizing the strange attractor. At its beginning, the surface splits into several branches (two in the present case). Each branch may be twisted by an integer number of half turns and/or wind around the other branches. All branches then rejoin each other along a common line (the *branch line*) where they are

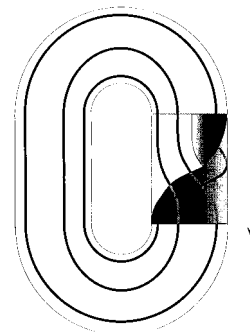


FIG. 5. The horseshoe template holding the x^2y period- $3T$ orbit. Its algebraic representation is given by the matrices in Eqs. (8).

superimposed in a certain order. The remaining part merely connects the branch line with the one where branches split off. It may display one or more full twists, whose number is called the global torsion of the template.

The horseshoe template is of particular interest not only because of its simplicity but also because it is the only one that has been, so far, clearly observed in experimental systems. It has been identified in optical systems, such as CO₂ lasers with modulated losses [7,8] or with a saturable absorber [6], a NMR laserlike oscillator [5], and other dynamical systems such as the Belousov-Zhabotinskii chemical reaction [2], an electrochemical reaction [3], or a vibrating string [4].

To relate experimentally measured invariants to the structure of the template, an algebraic description of the latter is needed. As proposed by Mindlin *et al.* [1,2], this can be achieved by defining two matrices, the $n \times n$ template matrix \mathcal{T} and the $1 \times n$ insertion matrix \mathcal{I} , where n is the number of branches of the template.

As we will see below, the topological organization of the chaotic regimes described in previous sections, corresponds to templates with two branches, and we therefore limit ourselves in the sequel to the $n=2$ case. Let us label the two branches x and y . We recall that each periodic orbit on the template can be given a unique symbolic name (which we write overlined) by listing the symbols of the branches that it successively visits. For example, the $\overline{x^2y^3}$ orbit visits branch x twice, then branch y thrice before returning to its starting point. In particular, there are two period-1 orbits \overline{x} and \overline{y} associated to the two branches of the template.

The template matrix is written out as

$$\mathcal{T} = \begin{pmatrix} t_x & 2l \\ 2l & t_y \end{pmatrix}, \quad (6)$$

where t_x (respectively, t_y) is the local torsion, in units of π , of the \overline{x} (respectively, \overline{y}) orbit, and thus the number of half-twists of the associated branch, and $l = lk(\overline{x}, \overline{y})$ is the linking number of the \overline{x} and \overline{y} orbits.

The insertion matrix \mathcal{I} reads

$$\mathcal{I} = (0 \quad m), \quad (7)$$

where $m=1$ (respectively, -1) if the y branch is above (respectively, below) the x branch on the branch line.

For example, the horseshoe structure with zero global torsion of Fig. 5 is described by the two following matrices:

$$\mathcal{T}_{hs} = \begin{pmatrix} 0 & 0 \\ 0 & 1 \end{pmatrix}, \quad (8a)$$

$$\mathcal{I}_{hs} = (0 \quad 1). \quad (8b)$$

The four numbers t_x , t_y , l , and m completely describe the structure of a two-branch template. As a result, the linking number of two periodic orbits with given symbolic sequences, as well as their self-linking numbers, can be expressed as functions of these numbers using techniques similar to those presented in Ref. [28]. In fact, these formulas are almost nearly linear, except for the presence of terms

involving $o(t_{x,y})$, where $o(t)$ indicates the parity of $t \in \mathbb{Z}$: $o(t)=1$ (respectively, 0) if t is odd (respectively, even).

Determining the template structure from the experimentally measured invariants thus amounts to equating the formulas yielding the invariants of some extracted orbits with the measured values, and then solving for the four unknowns t_x , t_y , l , and m . Four equations should, in principle, suffice. However, due to the presence of the $o(t_{x,y})$ terms, the computation is usually simpler when using a few more equations. As an example, we now determine the topological structure of the $C_{1/4}$ sample regime from the following five equations:

$$slk(\overline{xy}) = 2l + m = 7, \quad (9a)$$

$$lk(\overline{y}, \overline{xy}) = l + \frac{1}{2}[t_y + o(t_y)m] = 7, \quad (9b)$$

$$lk(\overline{y}, \overline{xyy}) = l + t_y = 10, \quad (9c)$$

$$lk(\overline{y}, \overline{xyyy}) = l + \frac{1}{2}[3t_y + o(t_y)m] = 14, \quad (9d)$$

$$lk(\overline{xy}, \overline{xyxy}) = 3l + m + t_x + \frac{1}{2}[t_y + o(t_y)m] = 20. \quad (9e)$$

Combining Eqs. (9b) and (9d) yields

$$t_y = lk(\overline{y}, \overline{xyyy}) - lk(\overline{y}, \overline{xy}) = 7. \quad (10)$$

Substituting this value of t_y in Eq. (9c) readily gives

$$l = 10 - t_y = 3. \quad (11)$$

Equation (9a) then indicates that

$$m = 7 - 2l = 1, \quad (12)$$

and, finally, Eq. (9e) yields the last unknown

$$t_x = 20 - 3l - m - \frac{1}{2}[t_y + o(t_y)m] = 6. \quad (13)$$

The template and insertion matrices are thus equal to

$$\mathcal{T} = \begin{pmatrix} 6 & 6 \\ 6 & 7 \end{pmatrix} = \underbrace{\begin{pmatrix} 0 & 0 \\ 0 & 1 \end{pmatrix}}_{\text{horseshoe}} + 3 \times \underbrace{\begin{pmatrix} 2 & 2 \\ 2 & 2 \end{pmatrix}}_{\text{global torsion}}$$

$$\mathcal{I} = (0 \quad 1), \quad (14b)$$

In Eq. (14a), the decomposition of \mathcal{T} shows that the corresponding template has a horseshoelike structure with a global torsion of 3. Indeed, as illustrated by Fig. 6, each element of a template matrix is increased by two when one full turn is added to the global torsion.

Note that we have found t_x and t_y to be even and odd, respectively. This could have been expected, as x and y , respectively, correspond to the branches of positive and negative slope of the 1D first return map. Hence, we could have slightly simplified the calculation by assuming from the beginning that $o(t_x)=0$ and $o(t_y)=1$. However, we wanted to stress that this piece of information is not strictly required.

As the reader may have noticed, we have used fewer topological invariants than have been measured. The remain-

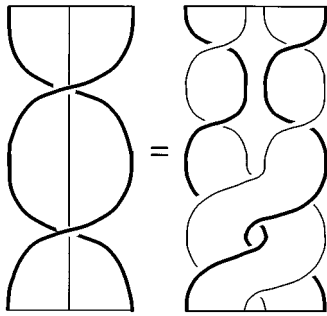


FIG. 6. Illustration of global torsion. Cutting the left ribbon in the middle yields the two ribbons on the right. It is easily seen that the contribution of the latter to the template matrix elements t_x , t_y , and $2l$ is equal to two.

ing ones can, thus, be used to validate the template by verifying that they are correctly predicted by the solution displayed in Eqs. (14). As an example,

$$lk(\overline{xyxy^2}, \overline{x^2y^2xy}) = 15l + 3t_x + \frac{9}{2}t_y + m\{6 - o(t_y)[\frac{1}{2} + o(t_x)]\}. \quad (15)$$

It can be easily checked that the experimentally measured value of 100 is obtained by substituting in Eq. (15) the values of t_x , t_y , l , and m given by Eqs. (14). In the same way, we have verified that all the unambiguous invariants listed in Tables II and III were correctly predicted by the template given in Eqs. (14).

The same procedure has been carried out for the chaotic attractors of the $C_{1/3}$ and $C_{1/2}$ windows and reveals horseshoe templates with global torsions of 2 and 1, respectively, [see Figs. 7(b) and 7(c)]

$$\mathcal{T}_{1/3} = \begin{pmatrix} 4 & 4 \\ 4 & 5 \end{pmatrix} = \begin{pmatrix} 0 & 0 \\ 0 & 1 \end{pmatrix} + 2 \times \begin{pmatrix} 2 & 2 \\ 2 & 2 \end{pmatrix}, \quad (16a)$$

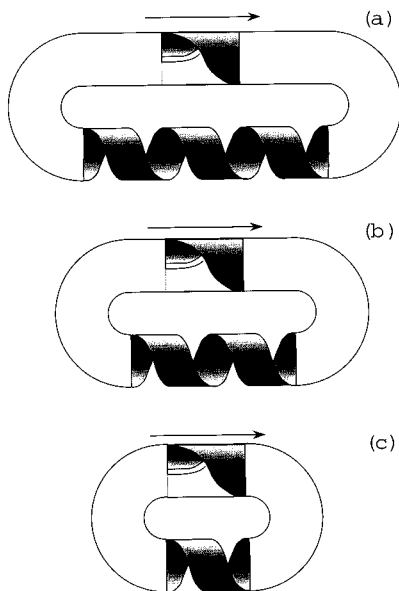


FIG. 7. Evolution of the template with the control parameter. (a) $C_{1/4}$ (b) $C_{1/3}$ (c) $C_{1/2}$.

$$\mathcal{T}_{1/3} = \begin{pmatrix} 0 & 1 \end{pmatrix} \quad (16b)$$

and

$$\mathcal{T}_{1/2} = \begin{pmatrix} 2 & 2 \\ 2 & 3 \end{pmatrix} = \begin{pmatrix} 0 & 0 \\ 0 & 1 \end{pmatrix} + 1 \times \begin{pmatrix} 2 & 2 \\ 2 & 2 \end{pmatrix}, \quad (17a)$$

$$\mathcal{T}_{1/2} = \begin{pmatrix} 0 & 1 \end{pmatrix}. \quad (17b)$$

It should be noted that for $\mathcal{T}_{1/2}$, due to the limited number of invariants, another template, with $t_y = 4$ instead of 3, is compatible with the measured topological invariants. We have, however, discarded this solution as (i) it does not reproduce the known parities of the two branches, (ii) a difference of two between the torsions of the two branches seems incompatible with the existence of a continuous flow.

It thus appears that chaotic regimes located inside the three chaotic regions $C_{1/2}$, $C_{1/3}$, and $C_{1/4}$ experience the same stretching and folding mechanisms as those described by Smale's horseshoe, but that they can be distinguished according to the global torsion of the template. The latter is closely connected to the ratio of the control parameter ω to the linear resonance frequency ω_r , as expected from the theoretical studies on nonlinear oscillators by Gilmore and McCallum [10]. The reader may verify that the existence of this global torsion is visible in Fig. 4 where global twists of, respectively, three, two, and one full turns can easily be seen.

V. CONCLUSION

We have analyzed the topological structure of chaotic attractors of a pump-modulated Nd-doped fiber laser for various values of the modulation frequency. Under the experimental conditions investigated, these chaotic regimes are found in islands $C_{1/n}$ located around the subharmonics ω_r/n ($n=2,3,4$) of the relaxation frequency ω_r .

Our main result is that the topological organization of the regimes found inside the $C_{1/n}$ region is not described by a simple horseshoe template, but by a horseshoe with a global torsion θ_g of $n-1$ in 2π units. This relation agrees with the theoretical study of the topology of nonlinear driven oscillators carried out by Gilmore and McCallum [10], and should accordingly hold in other experimental driven systems exhibiting chaos at subharmonic resonances. However, the present work provides, to our best knowledge, the first experimental illustration of this phenomenon, as well as the first experimental characterization of a system yielding different templates for different regions of the parameter space, in particular, templates with a nonzero global torsion.

Let us conclude by noting that more complex templates than those reported here should be found in other regions of parameter space. In the present study, indeed, the successive resonance tongues $C_{1/n}$ are separated by stable period- T behavior. When leaving the $C_{1/n}$ domain, all periodic orbits embedded in the strange attractor must be annihilated before the $C_{1/(n+1)}$ region is reached, because their invariants are

incompatible with the new topological organization. However, it is well known that resonance tongues may overlap when the modulation amplitude is sufficiently increased (see, e.g., [10]). In this case, some UPO of the $C_{1/n}$ domain can coexist in the same attractor with UPO of the $C_{1/(n+1)}$ region. As none of the above-mentioned templates can support simultaneously both types of orbits, this calls for the existence of more complex templates with more than two branches. The hope of observing such a template certainly

motivates further experimental investigations of the fiber laser and of other modulated class-*B* lasers.

ACKNOWLEDGMENTS

The Laboratoire de Spectroscopie Hertzienne is Unité de Recherche Associée au CNRS. The Centre d'Études et Recherches Lasers et Applications is supported by the Ministère Chargé de la Recherche, the Région Nord-Pas de Calais and the Fonds de Développement Économique des Régions.

-
- [1] G. B. Mindlin *et al.*, Phys. Rev. Lett. **64**, 2350 (1990).
 [2] G. B. Mindlin *et al.*, J. Nonlinear Sci. **1**, 147 (1991).
 [3] C. Letellier, L. L. Sceller, and J. L. Hudson, J. Phys. Chem. **99**, 7016 (1995).
 [4] N. B. Tufillaro *et al.*, Phys. Rev. E **51**, 164 (1995).
 [5] N. B. Tufillaro *et al.*, Phys. Rev. A **44**, 4786 (1991).
 [6] F. Papoff *et al.*, Phys. Rev. Lett. **68**, 1128 (1992).
 [7] M. Lefranc and P. Glorieux, Int. J. Bifurcation Chaos Appl. Sci. Eng. **3**, 643 (1993).
 [8] M. Lefranc *et al.*, Phys. Rev. Lett. **73**, 1364 (1994).
 [9] S. O. Firlé, M. A. Natiello, and M. Eiswirth, Phys. Rev. E **53**, 1257 (1995).
 [10] R. Gilmore and J. W. L. McCallum, Phys. Rev. E **51**, 935 (1995).
 [11] G. Boulant, M. Lefranc, S. Bielawski, and D. Derozier, Int. J. Bifurcation Chaos Appl. Sci. Eng. (to be published).
 [12] D. Pieroux and P. Mandel, Opt. Commun. **107**, 245 (1994).
 [13] Y. I. Khanin, *Principles of Laser Dynamics* (Elsevier, Amsterdam, 1995).
 [14] D. Auerbach *et al.*, Phys. Rev. Lett. **58**, 2387 (1987).
 [15] S. Bielawski, D. Derozier, and P. Glorieux, Phys. Rev. A **46**, 2811 (1992).
 [16] D. Derozier, S. Bielawski, and P. Glorieux, Opt. Commun. **83**, 97 (1991).
 [17] K. Briggs, Phys. Lett. A **151**, 27 (1990).
 [18] G. B. Mindlin and R. Gilmore, Physica D **58**, 229 (1992), special issue on Interpretation of Time Series from Nonlinear Dynamics.
 [19] L. H. Kaufmann, *Knots and Physics* (World Scientific, Singapore, 1991).
 [20] J. Guckenheimer and P. J. Holmes, *Nonlinear Oscillations, Dynamical Systems, and Bifurcations of Vector Fields* (Springer, Berlin, 1983).
 [21] J. S. Birman and R. F. Williams, Topology **22**, 47 (1983).
 [22] P. J. Holmes, in *New Directions in Dynamical Systems*, edited by T. Bedford and J. Swift (Cambridge University Press, Cambridge, 1988), pp. 150–191.
 [23] P. J. Holmes, Physica D **40**, 42 (1989).
 [24] H. G. Solari and R. Gilmore, Phys. Rev. A **37**, 3096 (1988).
 [25] N. B. Tufillaro, H. G. Solari, and R. Gilmore, Phys. Rev. A **41**, 5717 (1990).
 [26] M. Lefranc, D. Hennequin, and P. Glorieux, Phys. Lett. A **163**, 269 (1992).
 [27] B.-L. Hao, *Elementary Symbolic Dynamics and Chaos in Dissipative Systems* (World Scientific, Singapore, 1989).
 [28] N. B. Tufillaro, T. A. Abbott, and J. P. Reilly, *An Experimental Approach to Nonlinear Dynamics and Chaos* (Addison-Wesley, Reading, 1992).
 [29] J. L. Kaplan and J. A. Yorke, in *Functional Differential Equations and Approximation of Fixed Points*, edited by H. O. Walter and H.-O. Peitgen (Springer, Berlin, 1979), Vol. 730, pp. 204–227.